ACS APPLIED MATERIALS & INTERFACES

Research Article

Cite This: ACS Appl. Mater. Interfaces 2020, 12, 2095−2106

www.acsami.org

Enhanced Neural Regeneration with a Concomitant Treatment of Framework Nucleic Acid and Stem Cells in Spinal Cord Injury

Wenjuan Ma,[†] Yuxi Zhan,[†] Yuxin Zhang, Xueping Xie, Chenchen Mao, and Yunfeng Lin*

State Key Laboratory of Oral Diseases, National Clinical Research Center for Oral Diseases, West China Hospital of Stomatology, Sichuan University, Chengdu 610041, P. R. China

ABSTRACT: Spinal cord injury (SCI), began with a primary injury including contusion and compression, is a common disease caused by various pathogenesis. Characterized disruption of axons and irreversible loss of neurons in SCI, and further damage in spinal cord tissue caused by following secondary injuries, such as the formation of glial scar and inflammation, makes it even harder to recover for affected patients. Tetrahedral framework nucleic acid (tFNA), which possesses the capability of promoting neuroprotection and neuroregeneration in vitro, might alleviate the injuries, and facilitate the neural tissue regeneration in experimental animal models of SCI. Here, we developed a concomitant treatment of tFNA and neural stem cells (NSCs) for the synergistic therapy in treating the injury of the spinal cord. We first observed that tFNA could promote cell proliferation of NSCs then verified that the concomitant treatment of tFNA and NSCs showed the neuroprotective actions by increasing the survival of transplanted NSCs. Furthermore, the recovery of motor function and the tissue regeneration in the lesion site of the spinal cord achieved the best performance in the SCI rats treated with the combination of tFNA and NSCs than others, and the formation of glial scar was the least. Our findings provide novel evidence of a promising strategy for synergistic treatment of SCI in the future.

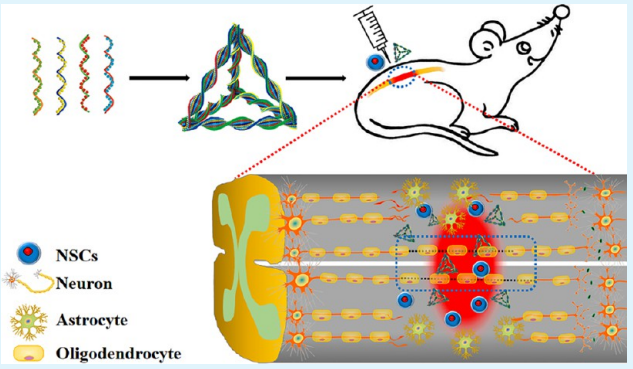

KEYWORDS: *spinal cord injury, tetrahedral framework nucleic acid, neural stem cells, translation, regeneration, animal model*

INTRODUCTION

Spinal cord injury (SCI), mostly caused by traumatic events in young males, is a damage to the spinal cord that will cause temporary or permanent functional changes.[1−4] The SCI could also resulted from nontraumatic diseases including infection, tumors, and degenerative disk diseases among older persons, making the incidence increase with aging.[5−7] As one of the common diseases for humans, the SCI can result in dramatic disability, thus causing poor life quality and serious socioeconomic burdens for affected individuals and families.[1,6−8] However, there are still no reliable medicines or therapeutics that could be effectively used to treat SCI till now.[1,9−11]

During SCI, the irreversible loss of neurons, the damages of vascular and blood-spinal cord barrier, and the disruption of axons in the wounded spinal cord are all big challenges to achieve functional recovery for patients.[1,9−11] These pathophysiological events can further trigger secondary injuries of normal tissue around the lesion such as excitotoxicity, formation of cystic cavities and hypertrophic scar, inflammation, and ischemia, which can lead to exacerbation of the injured site and spread damage that further impede the recovery of patients.[1,2,5,9−11]

Neuroprotection and neuroregeneration are the two main strategies for treating SCI currently.[2,5] Medicines for neuroprotection, such as epothilone B, dexamethasone, and methylprednisolone, are applied by preventing the extensive degeneration caused by secondary injury,[12−16] hence restricting the further damage of the spinal cord.[2,5,17,18] In contrast, the treatments for neuroregeneration, such as cell transplantation and tissue engineering, aim to recontribute the connections of injured neuronal tissues, promote axon and neuron regeneration, and recuperate the neural loss via the recellularization in the wounded site of the spinal cord.[1,9−11] Although these therapeutic options have been oberved with efficacy in treating SCI in previous studies, their applications in preclinical trials and clinical practice are still limited by high costs and low therapeutic efficiency in vivo.[1,8,11,19−21] Thereby, a therapeutic strategy with high biocompatibility and cost efficiency and combining effects of both neuroprotection and neuroregeneration simultaneously might be of great promise in the treatment of SCI.

The medications based on stem cell transplantation (SCT) gain increasing attention in treating nervous system diseases, including Parkinson's disease (PD), Alzheimer's disease (AD), and nervous system injury.[6−8,19−25] However, some studies demonstrated that therapies with only cell transplantation have

Received: October 23, 2019
Accepted: December 17, 2019
Published: December 17, 2019

DOI: 10.1021/acsami.9b19079
ACS Appl. Mater. Interfaces 2020, 12, 2095−2106

limitations of low cell survival rate, poor differentiation efficiency, and the unwarranted source security of transplanted cells.[6−8,19−21] In this context, the co-transplantation of stem cells with other cells or biomaterials, which could regulate the microenvironment and promote the survival rate and differentiation of neural stem cells (NSCs) with high safety and efficacy, was urgently needed for cell therapies in SCI.[8,19−21]

Tetrahedral framework nucleic acid (tFNA), a nanophase material with special nanostructure, has been widely investigated in various biological medical applications, including biosensors, delivery system of drugs, and disease-targeted diagnosis.[26−38] The functions of tFNA have also been studied in stem cell engineering and in treating nervous system diseases.[39−41] For instance, previous studies have demonstrated that tFNA could promote NSCs to proliferate, migrate, and differentiate into neurons[39,40] and accelerate cell self-renewal of chondrocytes.[42,43] It has also been proven that tFNA could avoid the neurological damage caused by Aβ protein in the AD cell model[41] and possessed anti-inflammatory and antioxidative effects on macrophages.[44] Therefore, the tFNA might be a promising regenerative medicine in tissue engineering and a suitable candidate for co-transplantation therapeutic strategy with stem cells in treating SCI.

Thus, in this study, we examined the hypothesis that co-transplantation of NSCs and tFNA via a direct intramedullary transplantation would have better performance in treating and promoting higher transplanted cell survival at the injured site of the SCI animal model than only NSCs or only tFNA (Scheme 1). The combined NSCs and tFNA treatment was also hypothesized to enhance NSCs in proliferating and differentiating into neurons and oligodendrocytes but not astrocytes, which might be better to avoid the formation of glial scar for the recovery of nerve tissue (Scheme 1).

Scheme 1. Schematic Diagram Depicting the Application of Concomitant Treatment of tFNA and NSCs in Spinal Cord Injury (SCI)[a]

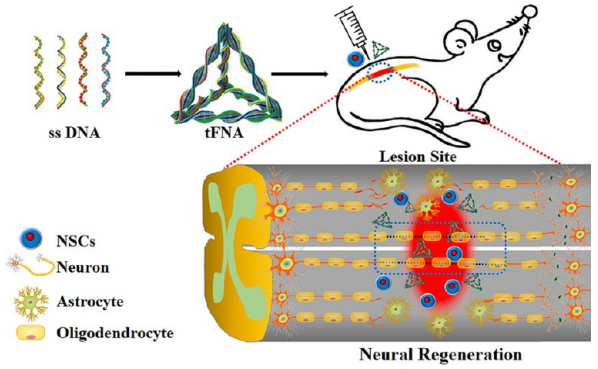

[a]tFNA could promote NSCs differentiate into neurons and oligodendrocytes but not astrocytes, which indicated that the concomitant treatment of tFNA and NSCs possessed the excellent neural tissue regeneration effects. The rats treated with tFNA/NSCs exhibited much better motor functional recovery and tissue regeneration.

RESULTS AND DISCUSSION

Fabrication and Characterization of tFNA. In Figure 1A, the schematic diagram showed the procedures of the synthesis of tFNA. In Figure 1B, the results of capillary gel electrophoresis (CGE) indicated that the four single-stranded DNA (ssDNA) could form the tFNA. The results of polyacrylamide gel electrophoresis (PAGE) shown in Figure 1C suggested successful generation of tFNA. The size of tFNA measured by dynamic light scattering (DLS) was 11.213 ± 0.654 nm, and the polymer dispersity index (PDI) result of tFNA was 0.356 ± 0.162 (Figure 1D). The size of tFNA tested by transmission electron microscopy (TEM) was approximately 10.0 nm (Figure 1). The result of atomic force microscopy (AFM) is shown in Figure 1F, which revealed that the dimension of tFNA was approximately 10.0 nm in length and 4.0 nm in height. The results above showed that the tFNA could be generated successfully, which is an essential prerequisite for further experiments and investigations in the current study.

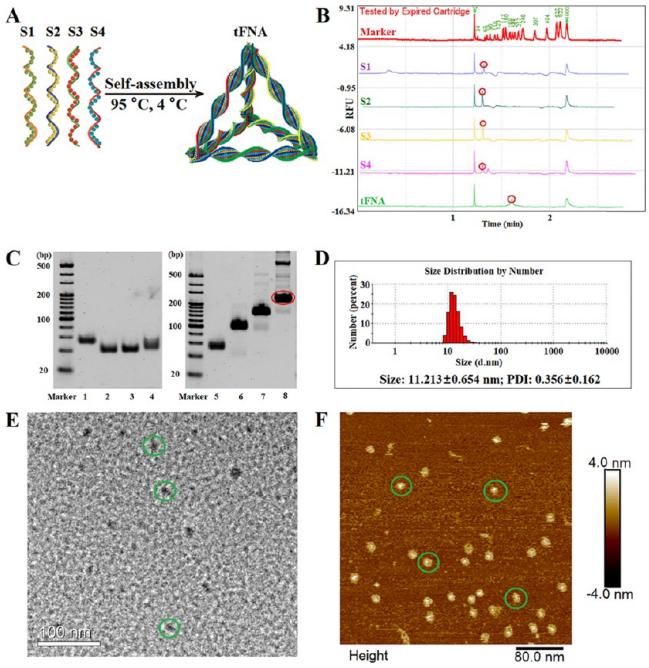

Figure 1. Generation and characterization of tFNA. (A) Schematic illustration of the synthetic process of tFNA. (B) Confirmation of the successful synthesis of tFNA by capillary gel electrophoresis (CGE). (C) Polyacrylamide gel electrophoresis (PAGE) was used to prove the successful generation of tFNA. Line 1, S1. Line 2, S2. Line 3, S3. Line 4, S4. Line 5, S1. Line 6, S1 + S2. Line 7, S1 + S2 + S3. Line 8, S1 + S2 + S3 + S4, tFNA. (D) Dynamic light scattering (DLS) measurement statistics of tFNA. The size distribution result of tFNA was 11.213 ± 0.654 nm (n = 3). The PDI result of tFNA was 0.356 ± 0.162 (n = 3). (E) Transmission electron microscopy (TEM) image of tFNA. Scale bar is 100 nm. (F) Atomic force microscopy (AFM) image of tFNA. Scale bar is 80.0 nm.

Given that the nature of tFNA is nucleic acid, which maintains high biocompatibility and safety, the tFNA might also be used in loading and delivering some medicines specifically to the targeted nidus in future studies, which could enhance the treatment effects of various medicines.

Cell Culture and Identification. From the results shown in Figure 2A, we found that the isolation of NSCs could be separated from the rat brain, and the neural spheres were formed after the cells cultured for several days, suggesting the successful cell self-renewal of NSCs during in vitro culture. To confirm that NSCs were primitive, Nestin protein was tested. As shown in Figure 2B, we could tell that the Nestin was

DOI: 10.1021/acsami.9b19079
ACS Appl. Mater. Interfaces 2020, 12, 2095−2106

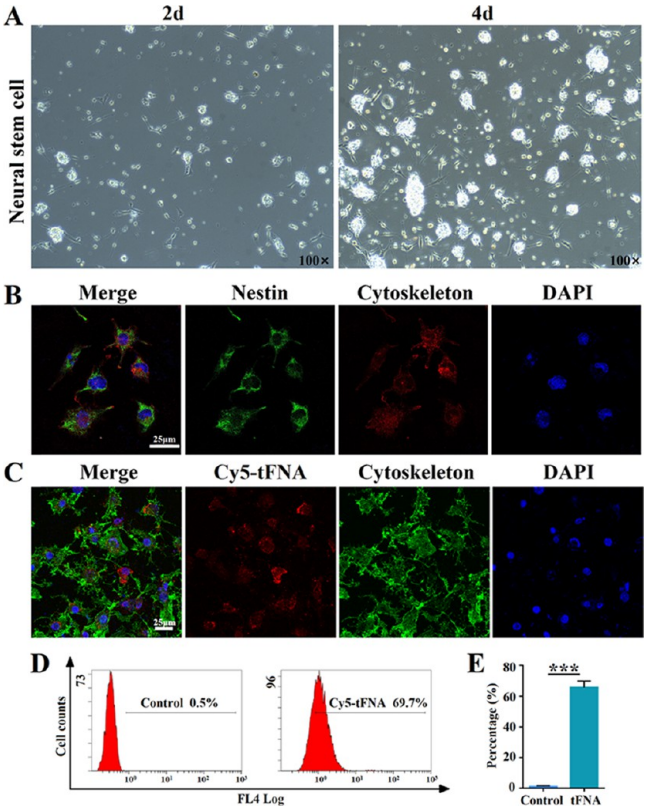

Figure 2. Cell culture and identification of NSCs and cellular uptake of tFNA by NSCs. (A) Culture of isolated NSCs from fetal rats. (B) Immunofluorescence images of NSCs (Nestin: green, cytoskeleton: red, and nucleus: blue). Scale bars are 25 μm. (C) Confocal laser scanning microscopy images show the NSC uptake of Cy5-tFNA (Cy5-tFNA: red, cytoskeleton: red, and nucleus: blue). Scale bars are 25 μm. (D) Flow cytometry analysis of cellular uptake rate in NSCs after being treated with 250 nM Cy5-FNA for 12 h. (E) Quantitative analysis of flow cytometry. Data are presented as mean ± SD (n = 3). Statistical analysis: ***p < 0.001.

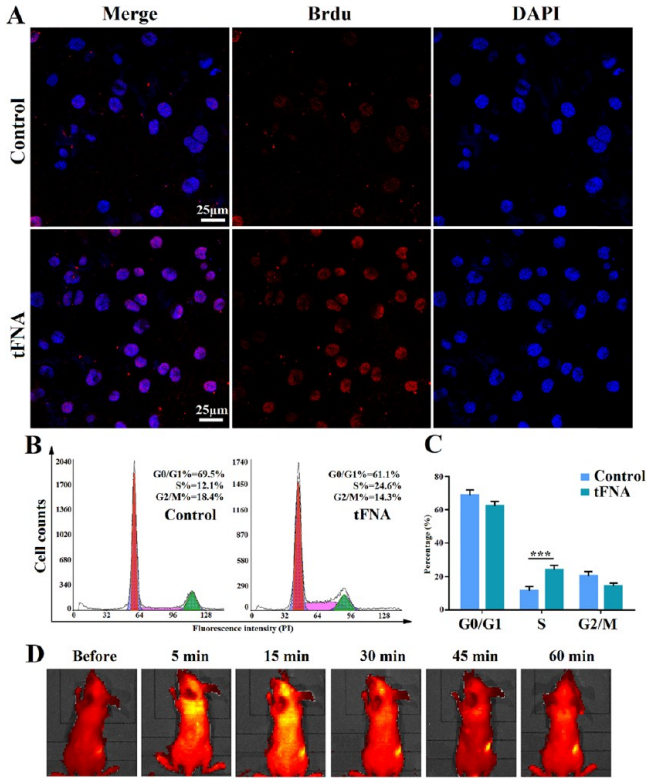

Figure 3. Cell proliferation effects of tFNA on NSCs and the blood circulation of tFNA in vivo. (A) Confocal laser scanning microscopy images show the tFNA effect on cell proliferation by Brdu incorporation. The cell proportion of Brdu-positive was higher in the tFNA-treated group (Brdu: red, and nucleus: blue). Scale bars are 25 μm. (B) Flow cytometry analysis of cell cycle after NSCs treated with tFNA. (C) Analysis data of cell cycle distribution. Data are presented as mean ± SD (n = 3). Statistical analysis: ***p < 0.001. (D) Representative fluorescence imaging of Babl/c nude mice after the injection of Cy5-tFNA (n = 3).

expressed highly in NSCs, indicating that the cells were not differentiated.

Cellular Uptake of tFNA. From the in vitro experiments of cellular uptake of tFNA (Figure 2C), the results indicated that the Cy5-tFNA could be internalized by NSCs. From the results of flow cytometry (Figure 2D,E), it showed that more than 60% NSCs could ingest Cy5-tFNA after incubation with Cy5-tFNA for 12 h. The cellular uptake of tFNA is the prerequisite for tFNA to exert its effects on NSCs. The tFNA will also be developed as an excellent drug delivery system in our further study.

Cell Proliferation Assay. Previous studies have reported that tFNA could facilitate the self-renewal of NE-4C cells and PC12 cells. In this study, we used Brdu straining and flow cytometry to examine whether tFNA could enhance the proliferation of primary NSCs. In Figure 3A, it shows that the DNA in NSCs after being treated with tFNA for 24 h had more replications than that without giving tFNA. As presented in Figure 3B,C, the flow cytometry results suggested that tFNA could increase the cell number of phase S significantly. From the results above, we could tell that the cell proliferation of NSCs could be promoted after being exposed to tFNA, which indicated that tFNA had the potential in neural tissue regeneration.

Blood Circulation Time of tFNA. From the results shown in Figure 3D, we could find that the distribution of Cy5-tFNA in vivo kept changing with time, and the blood circulation time was approximately 1 h. It showed that the tFNA did not aggregate in the spinal cord; therefore, we used subdural injection of tFNA in this study.

Enhanced Functional Recovery after SCI by Using tFNA and NSCs. To evaluate whether tFNA could effectively improve the functional recovery after SCI, adult Sprague–Dawley (SD) rats were subjected to lateral hemisection at the T9 and typically treated with a single application of normal saline (NS), free tFNA, free NSCs, and NSCs/tFNA. The functional recovery in SCI was evaluated by Basso–Beattie–Bresnahan (BBB) scores, a measure that could reflect the motor and sensory functional remodeling.[45,46] After SCI operation, all experimental rat hindlimbs were immediately paralyzed as expected. There was no significant difference in BBB scores among all rat groups in 1 week after the operation. However, the BBB scores of rats treated with NSCs/tFNA improved significantly after 2 week treatment and kept increasing thereafter (Figure 4A and Table 2). To further observe the long-term recovery of motor function, BBB scores were also compared among groups at the ends of fourth and eight week after SCI. Relative to the free NSCs-treated or free tFNA-treated group, the significantly higher BBB scores in

DOI: 10.1021/acsami.9b19079
ACS Appl. Mater. Interfaces 2020, 12, 2095–2106

Table 1. Base Sequence of Each ssDNA

ssDNA	base sequence	direction
Cy5-S1	Cy5-ATTTATCACCCGCCATAGTAGACGTATCACCAGGCAGTTGAGACGAACATTCCTAAGTCTGAA	5′→3′
S1	ATTTATCACCCGCCATAGTAGACGTATCACCAGGCAGTTGAGACGAACATTCCTAAGTCTGAA	5′→3′
S2	ACATGCGAGGGTCCAATACCGACGATTACAGCTTGCTACACGATTCAGACTTAGGAATGTTCG	5′→3′
S3	ACTACTATGGCGGGTGATAAAACGTGTAGCAAGCTGTAATCGACGGGAAGAGCATGCCCATCC	5′→3′
S4	ACGGTATTGGACCCTCGCATGACTCAACTGCCTGGTGATACGAGGATGGGCATGCTCTTCCCG	5′→3′

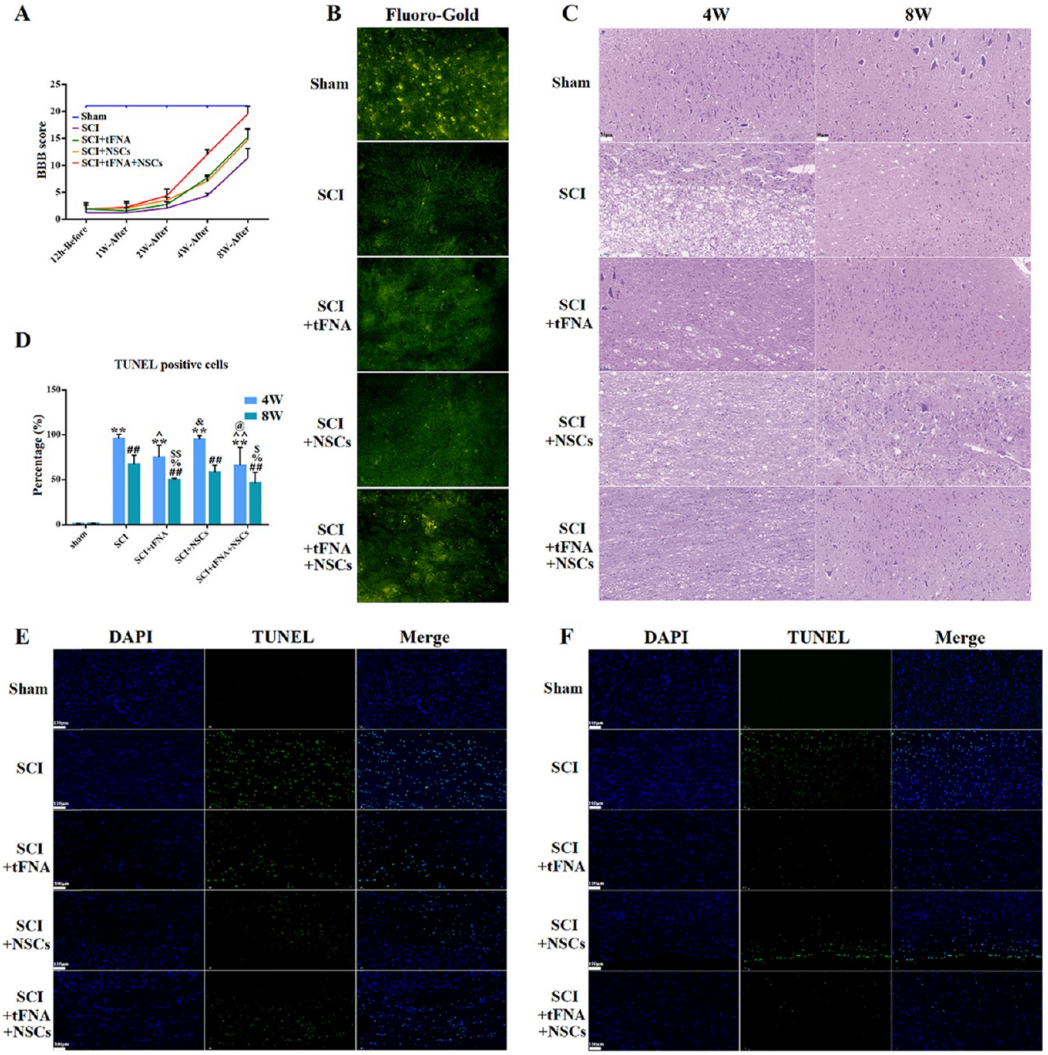

Figure 4. The concomitant treatment of tFNA and NSCs promotes motor functional recovery in rats after SCI. (A) BBB scores for each group at determined points (n = 10). (B) Images of amino cupric silver staining (n = 3). (C) H&E staining of the injured tissue around the SCI model rats at determined time points (n = 3). Scale bars are 50 μm. (D) Statistical analysis of the percentage of TUNEL-positive cells in the lesion sites of each group. Data are presented as mean ± SD (n = 5). Statistical analysis: $^{**}p < 0.01$ versus sham (4W); $^{\wedge}p < 0.05$, $^{\wedge\wedge}p < 0.01$ versus SCI (4W); $^{\&}p < 0.05$ versus SCI+tFNA (4W); $^{@}p < 0.05$ versus SCI+NSCs (4W); $^{\#\#}p < 0.01$ versus sham (8W); $^{\%}p < 0.05$ versus SCI (8W); $^{\$}p < 0.05$, $^{\$\$}p < 0.01$ versus SCI+NSCs (8W). (E) TUNEL staining in the lesion sites of SCI model rats after 4 week treatment. Scale bars are 100 μm. (F) TUNEL staining in the lesion sites of SCI model rats after 8 week treatment. Scale bars are 100 μm.

Table 2. BBB Scores for Each Group at Determined Points

group/time	12h-before	1W-after	2W-after	4W-after	8W-after
sham	19.67 ± 0.33	20.78 ± 0.17	21.00 ± 0.00	20.00 ± 0.37	20.33 ± 0.33
SCI	1.00 ± 0.17^{a}	1.33 ± 0.17^{a}	2.00 ± 0.29^{abc}	4.33 ± 0.21^{abcd}	10.50 ± 0.34^{abcde}
SCI+tFNA	1.33 ± 0.17^{a}	1.56 ± 0.18^{a}	2.33 ± 0.17^{abc}	7.67 ± 0.21^{abcdf}	15.33 ± 0.31^{aabcdef}
SCI+NSCs	1.44 ± 0.18^{a}	1.78 ± 0.22^{a}	3.56 ± 0.24^{abcfg}	7.50 ± 0.22^{abcdf}	15.83 ± 0.33^{abcdefg}
SCI+tFNA+NSCs	1.11 ± 0.20^{a}	1.67 ± 0.24^{a}	4.67 ± 0.41^{abcfgh}	12.00 ± 0.37^{abcfgh}	18.67 ± 0.31^{bcdefgh}

^{a}versus sham. ^{b}versus 12-before. ^{c}versus 1W-after. ^{d}versus 2W-after. ^{e}versus 4W-after. ^{f}versus SCI+PBS. ^{g}versus SCI+DNA. ^{h}versus SCI+NSCs.

DOI: 10.1021/acsami.9b19079
ACS Appl. Mater. Interfaces 2020, 12, 2095−2106

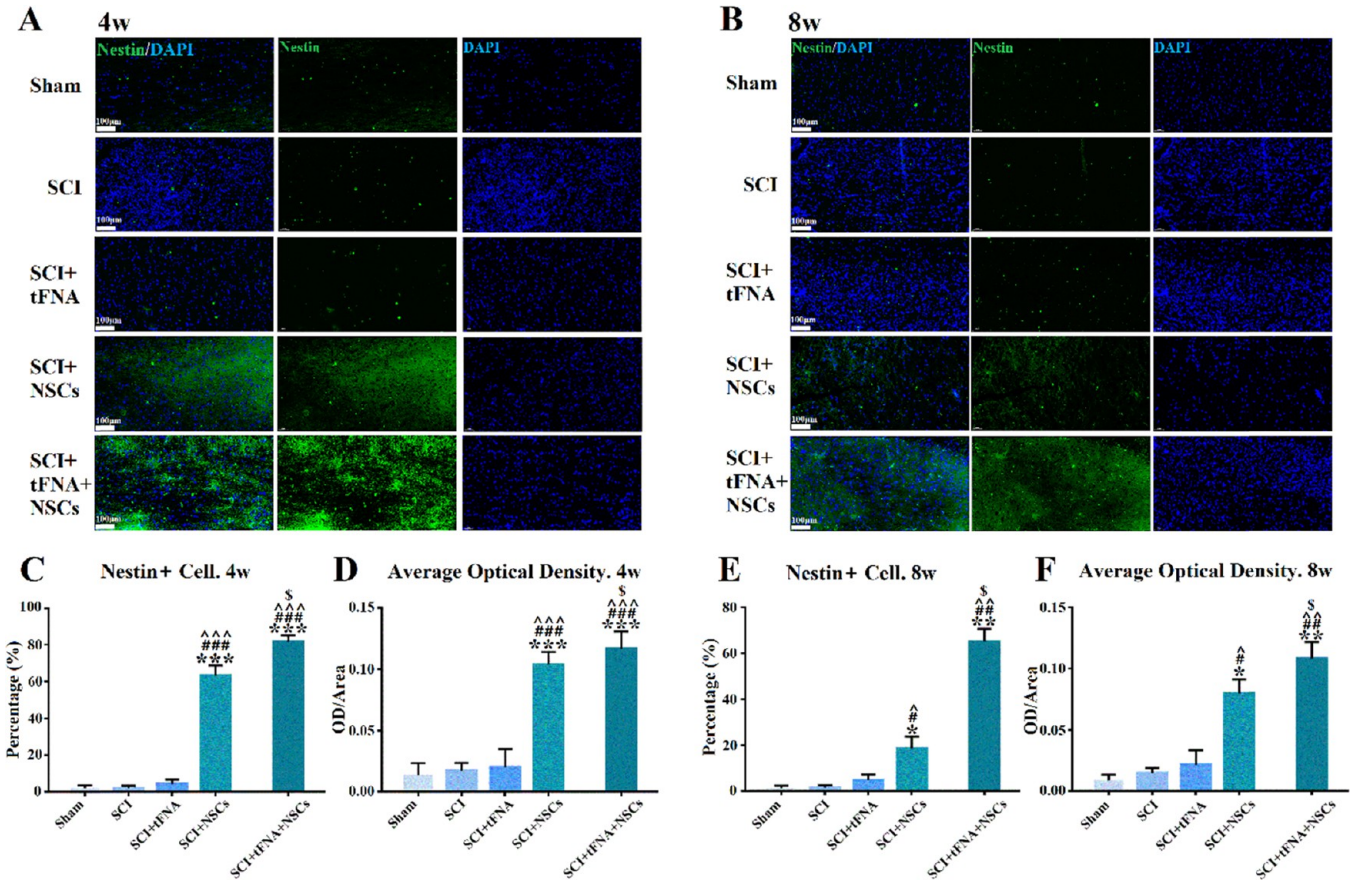

Figure 5. Immunohistochemistry of Nestin protein in the lesion sites of each group. (A) Immunohistochemistry images of Nestin protein in the lesion sites of SCI model rats after 4 week treatment. Scale bars are 100 μm. (B) Immunohistochemistry images of Nestin protein in the lesion sites of SCI model rats after 8 week treatment. Scale bars are 100 μm. (C) Statistical analysis of the percentage of Nestin-positive cells in the lesion sites of SCI model rats after 4 week treatment. Data are presented as mean ± SD (n = 3). Statistical analysis: $^{***}p < 0.001$ versus sham; $^{\#\#\#}p < 0.001$ versus SCI; $^{\wedge\wedge\wedge}p < 0.001$ versus SCI+tFNA; $^{\$}p < 0.05$ versus SCI+NSCs. (D) Quantification of the average optical density of the Nestin in the lesion sites of SCI model rats after 4 week treatment. Data are presented as mean ± SD (n = 3). Statistical analysis: $^{***}p < 0.001$ versus sham; $^{\#\#\#}p < 0.001$ versus SCI; $^{\wedge\wedge\wedge}p < 0.001$ versus SCI+tFNA; $^{\$}p < 0.05$ versus SCI+NSCs. (E) Statistical analysis of the percentage of Nestin-positive cells in the lesion sites of SCI model rats after 8 week treatment. Data are presented as mean ± SD (n = 3). Statistical analysis: $^{*}p < 0.05$, $^{**}p < 0.01$ versus sham; $^{\#}p < 0.05$, $^{\#\#}p < 0.01$ versus SCI; $^{\wedge}p < 0.05$, $^{\wedge\wedge}p < 0.01$ versus SCI+tFNA; $^{\$}p < 0.05$ versus SCI+NSCs. (F) Quantification of the average optical density of the Nestin in the lesion sites of SCI model rats after 8 week treatment. Data are presented as mean ± SD (n = 3). Statistical analysis: $^{*}p < 0.05$, $^{**}p < 0.01$ versus sham; $^{\#}p < 0.05$, $^{\#\#}p < 0.01$ versus SCI; $^{\wedge}p < 0.05$, $^{\wedge\wedge}p < 0.01$ versus SCI+tFNA; $^{\$}p < 0.05$ versus SCI+NSCs.

NSCs/tFNA-treated rat group at the two longitudinal time points indicated that the combined treatment of NSCs and tFNA had better therapeutic effects on SCI modeled rats (Figure 4A and Table 2). In the following comparisons, BBB scores did not differ between the free tFNA-treated group and free NSCs-treated group, but the scores in these two groups were higher than those in the control (NS-treated) rat group. This was seen at all time points.

To further investigate the functional recovery of nerve conduction at the injured site with different treatments, the amino cupric silver staining was used. As shown in Figure 4B, the NSCs/tFNA-treated rat group had better functional recovery of nerve conduction than other groups significantly. However, there was no significant difference between free NSCs-treated and free tFNA-treated groups, indicating that the tFNA and NSCs might have comparable effects on the transplantation of NSCs. In Figure 4C, the results of the H&E (hematoxylin and eosin) stained sections suggested that the tissue in the NSCs/tFNA-treated group had much less necrosis than other groups, also suggesting a better regeneration of neural tissue with the combined treatment of tFNA and NSCs.

To characterize the cell survival rate of transplanted NSCs, the TUNEL staining of the injured site was also conducted at the ends of fourth and eight week after SCI.[47−49] As shown in Figure 4D−F, the TUNEL staining indicated that more NSCs could survive in the NSCs/tFNA-treated group. There was no difference between the free NSCs-treated group and free tFNA-treated group in the cell survival rate, but that of NSCs in these two groups was much higher than the control group. These results indicated that tFNA could increase the survival rate of NSCs, which was vital for the transplanted cells.

Our findings revealed that tFNA had neuroprotective effects on the transplanted NSCs by increasing the survival rate of cells. The recovery of nerve conduction and the tissue regeneration of H&E indicated that tFNA could facilitate the transplanted NSCs to rebuild and recover. The functional recovery as rated by BBB scores suggested that tFNA was a promising biological material in tissue engineering for regenerative medicine.[1,9,45,46]

DOI: 10.1021/acsami.9b19079
ACS Appl. Mater. Interfaces 2020, 12, 2095−2106

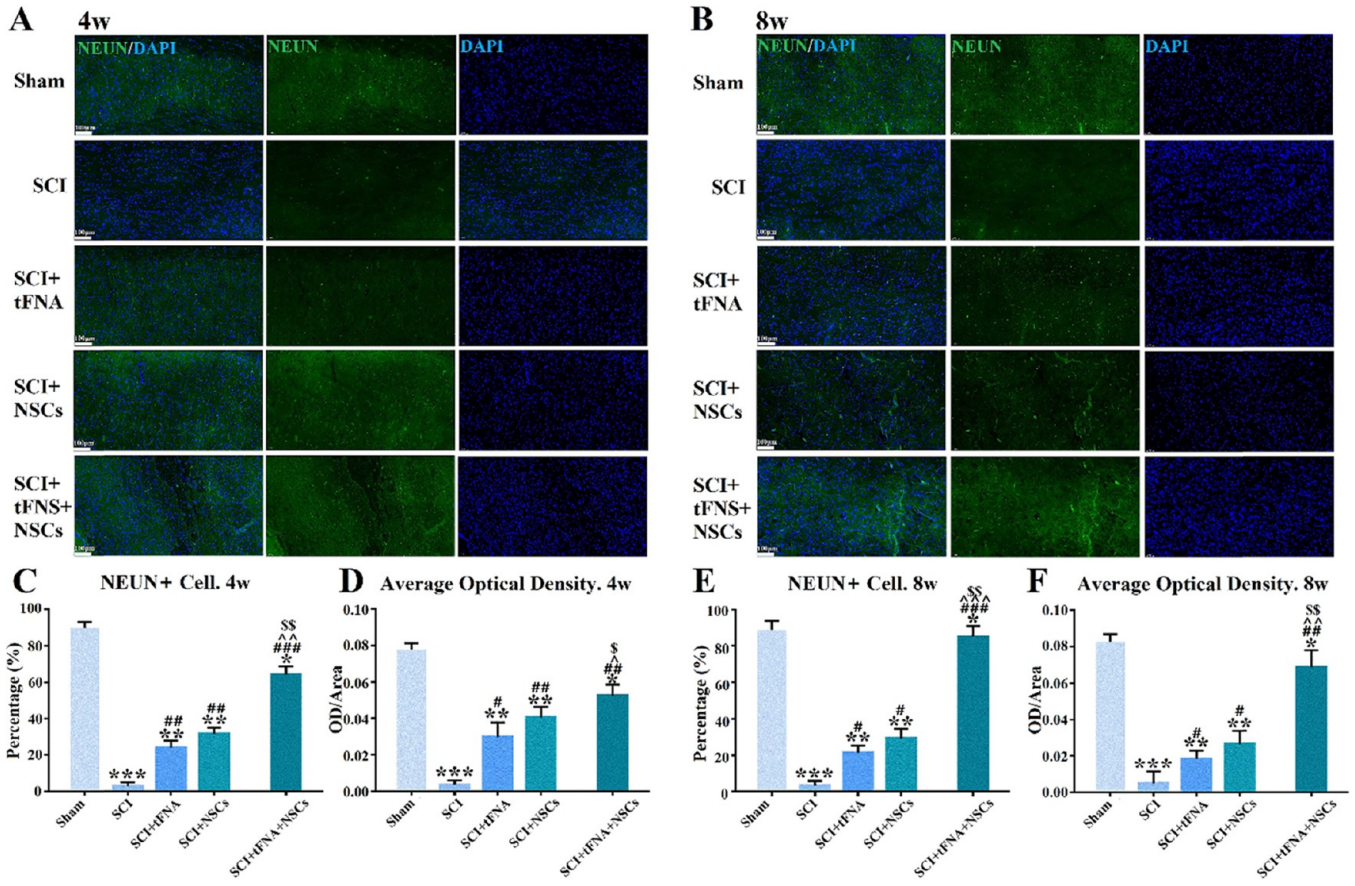

Figure 6. Immunohistochemistry of NEUN protein in the lesion sites of each group. (A) Immunohistochemistry images of NEUN protein in the lesion sites of SCI model rats after 4 week treatment. Scale bars are 100 μm. (B) Immunohistochemistry images of NEUN protein in the lesion sites of SCI model rats after 8 week treatment. Scale bars are 100 μm. (C) Statistical analysis of the percentage of NEUN-positive cells in the lesion sites of SCI model rats after 4 week treatment. Data are presented as mean ± SD (n = 3). Statistical analysis: $^{*}p < 0.05$, $^{**}p < 0.01$, $^{***}p < 0.001$ versus sham; $^{\#\#}p < 0.01$, $^{\#\#\#}p < 0.001$ versus SCI; $\wedge\wedge p < 0.01$ versus SCI+tFNA; $^{\$\$}p < 0.01$ versus SCI+NSCs. (D) Quantification of the average optical density of the NEUN in the lesion sites of SCI model rats after 4 week treatment. Data are presented as mean ± SD (n = 3). Statistical analysis: $^{*}p < 0.05$, $^{**}p < 0.01$, $^{***}p < 0.001$ versus sham; $^{\#}p < 0.05$, $^{\#\#}p < 0.01$ versus SCI; $\wedge p < 0.05$ versus SCI+tFNA; $^{\$}p < 0.05$ versus SCI+NSCs. (E) Statistical analysis of the percentage of NEUN-positive cells in the lesion sites of SCI model rats after 8 week treatment. Data are presented as mean ± SD (n = 3). Statistical analysis: $^{*}p < 0.05$, $^{**}p < 0.01$, $^{***}p < 0.001$ versus sham; $^{\#}p < 0.05$, $^{\#\#\#}p < 0.001$ versus SCI; $\wedge\wedge\wedge p < 0.001$ versus SCI +tFNA; $^{\$\$}p < 0.01$ versus SCI+NSCs. (F) Quantification of the average optical density of the NEUN in the lesion sites of SCI model rats after 8 week treatment. Data are presented as mean ± SD (n = 3). Statistical analysis: $^{*}p < 0.05$, $^{**}p < 0.01$, $^{***}p < 0.001$ versus sham; $^{\#}p < 0.05$, $^{\#\#}p < 0.01$ versus SCI; $\wedge\wedge p < 0.01$ versus SCI+tFNA; $^{\$\$}p < 0.01$ versus SCI+NSCs.

The Differentiation of Transplanted NSCs. To observe the differentiation of transplanted NSCs, the immunohistochemistry was used. From the results shown in Figure 5, the Nestin-positive tissue was more in the NSCs/tFNA-treated group than other groups after 4 week and 8 week treatment of SCI.[50−52] More Nestin-positive tissue meant more NSC survival or proliferation, which indicated that tFNA could enhance the cell proliferation and survival of NSCs in vivo. The proliferation of transplanted NSCs is critical for the tissue regeneration. In Figure 6, the results suggested that the Neun-positive cells were obvious in the sham group and NSCs/tFNA-treated group. However, in the control group and tFNA-treated group, the tissue expression of Neun was lower than other groups. The results demonstrated that the tFNA could promote transplanted NSCs and differentiate into neurons after being treated with NSCs/tFNA. From the results of Figures 5 and 6, we could draw the conclusion that the NSCs/tFNA-treated group had better tissue regeneration and functional recovery.

In Figure 7, the expression of glial fibrillary acidic protein (GFAP) was the highest in the control group than other experiment groups, and the expression of GFAP in the NSCs/tFNA-treated group was the lowest, indicating that tFNA could inhibit NSCs to differentiate into astrocytes, which was consistent with results of the in vitro experiment. Previous studies have demonstrated that astrocytes could form the glial scar after SCI, which was one of the significant factors affecting regeneration of nerve fiber and neuron.[1,2,53−55] Therefore, the results of Figure 7 suggested that the tFNA could enhance the tissue regeneration by inhibiting the formation of glial scar in the group treated with tFNA and that the tFNA might have the synergistic effects on NSCs in treating SCI.

In Figure 8, the expression of MBP, a marker protein expressed in oligodendrocytes,[56] was more obvious in the NSCs/tFNA-treated group than other groups. The regeneration of oligodendrocytes can reestablish myelin sheaths and restore the carry signal function of nerve cells. These results indicated that tFNA could promote the transplanted NSCs and differentiate into oligodendrocytes in the NSCs/tFNA-treated

DOI: 10.1021/acsami.9b19079
ACS Appl. Mater. Interfaces 2020, 12, 2095−2106

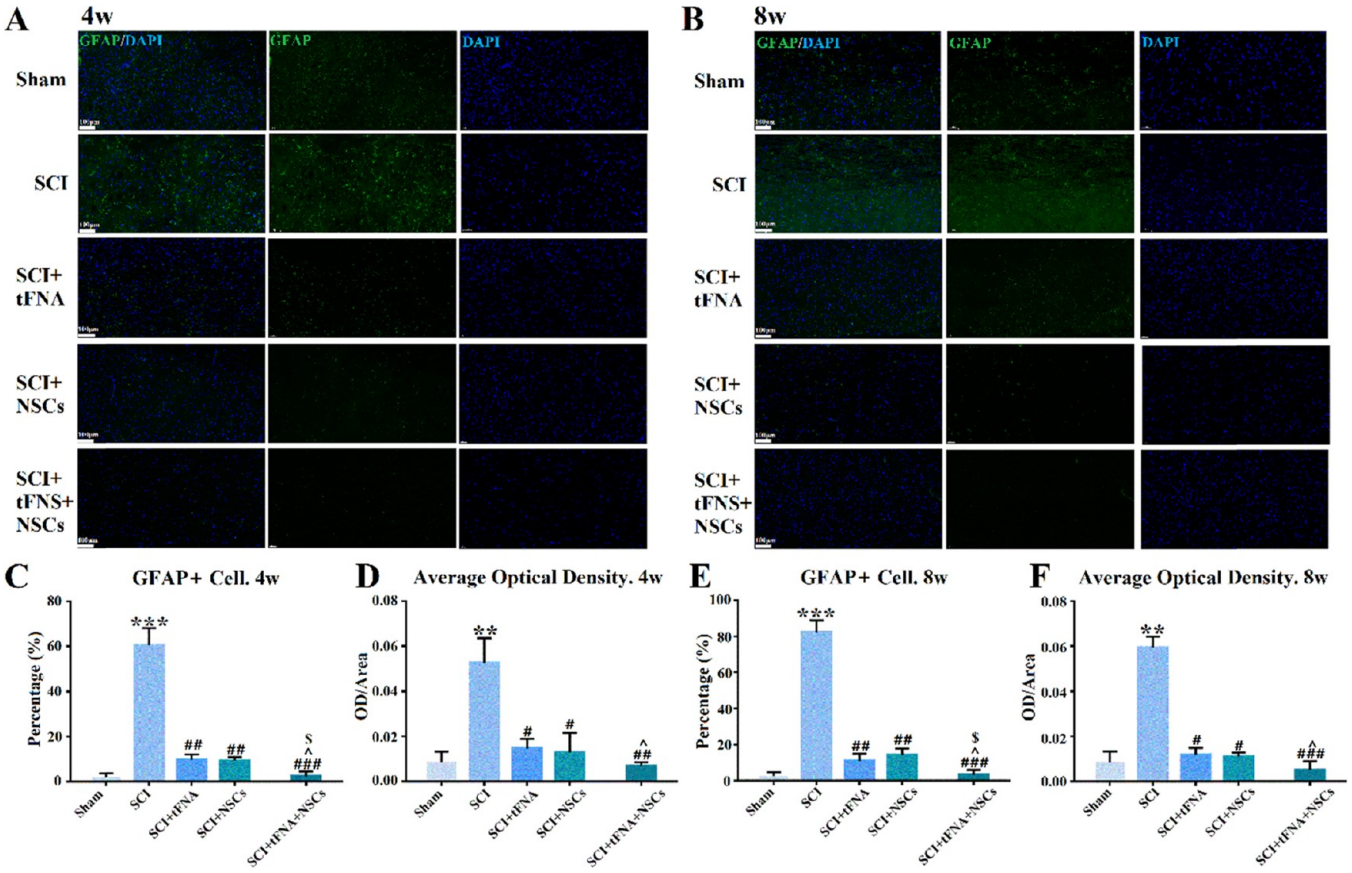

Figure 7. Immunohistochemistry of GFAP protein in the lesion sites of each group. (A) Immunohistochemistry images of GFAP protein in the lesion sites of SCI model rats after 4 week treatment. Scale bars are 100 μm. (B) Immunohistochemistry images of GFAP protein in the lesion sites of SCI model rats after 8 week treatment. Scale bars are 100 μm. (C) Statistical analysis of the percentage of GFAP-positive cells in the lesion sites of SCI model rats after 4 week treatment. Data are presented as mean ± SD (n = 3). Statistical analysis: $^{***}p < 0.001$ versus sham; $^{\#\#}p < 0.01$, $^{\#\#\#}p < 0.001$ versus SCI; $^{\wedge}p < 0.05$ versus SCI+tFNA; $^{\$}p < 0.05$ versus SCI+NSCs. (D) Quantification of the average optical density of the GFAP in the lesion sites of SCI model rats after 4 week treatment. Data are presented as mean ± SD (n = 3). Statistical analysis: $^{**}p < 0.01$ versus sham; $^{\#}p < 0.05$, $^{\#\#}p < 0.01$ versus SCI; $^{\wedge}p < 0.05$ versus SCI+tFNA. (E) Statistical analysis of the percentage of GFAP-positive cells in the lesion sites of SCI model rats after 8 week treatment. Data are presented as mean ± SD (n = 3). Statistical analysis: $^{***}p < 0.001$ versus sham; $^{\#\#}p < 0.01$, $^{\#\#\#}p < 0.001$ versus SCI; $^{\wedge}p < 0.05$ versus SCI+tFNA; $^{\$}p < 0.05$ versus SCI+NSCs. (F) Quantification of the average optical density of the GFAP in the lesion sites of SCI model rats after 8 week treatment. Data are presented as mean ± SD (n = 3). Statistical analysis: $^{**}p < 0.01$ versus sham; $^{\#}p < 0.05$, $^{\#\#\#}p < 0.001$ versus SCI; $^{\wedge}p < 0.05$ versus SCI+tFNA.

group, which was significant for the neurons to manifest their function. However, the expression of MBP did not differ between the free tFNA-treated group and the free NSCs-treated group.

Finally, we found that the tFNA could enhance the transplanted NSCs in proliferating and differentiating into neurons and oligodendrocytes, while the astrocytes were scarce at injured sites of SCI. The results indicated that the tFNA could promote the regeneration in injured sites after the co-transplantation of NSCs and tFNA and confirmed that the tFNA could facilitate the neural tissue formation in the injured spinal cord. However, our current study is somewhat superficial, and some limitations are noteworthy when interpreting our findings: (i) other detection methods should be used in this study to support these conclusions, such as the dorsal view of representative spinal cords of different groups, and the typical MRI (magnetic resonance imaging) images of all spinal cords, which were limited by experiment conditions; (ii) more physiological changes caused by SCI should be measured; (iii) the tissue regeneration effects of the combined treatment of NSCs and tFNA need to be confirmed by more experiments on different animal models to replicate the neuroprotective and neuroregenerative effects of tFNA; and (iv) the tFNA might be modified by other medicines to further enhance the effects of neuroprotection and neuroregeneration. In spite of these limitations, the current work shows promising evidence about neuroprotective and neuroregenerative effects of tFNA when co-transplanted with NSCs. Although clinical application of this combined tFNA and NSCs therapeutic strategy still requires further investigation, our study may initiate a significant step toward developing a new biomedicine to treat SCI.

CONCLUSIONS

In conclusion, our study first demonstrated that the tFNA could be taken into NSCs and could promote primary NSC proliferation. In the further in vivo experiments, we found the tFNA could increase the survival of transplanted NSCs and promote them to differentiate into neurons and oligodendrocytes. More importantly, the combined use of tFNA and NSCs showed better performance than each of them in inhibiting the transplanted NSCs to differentiate into

DOI: 10.1021/acsami.9b19079
ACS Appl. Mater. Interfaces 2020, 12, 2095−2106

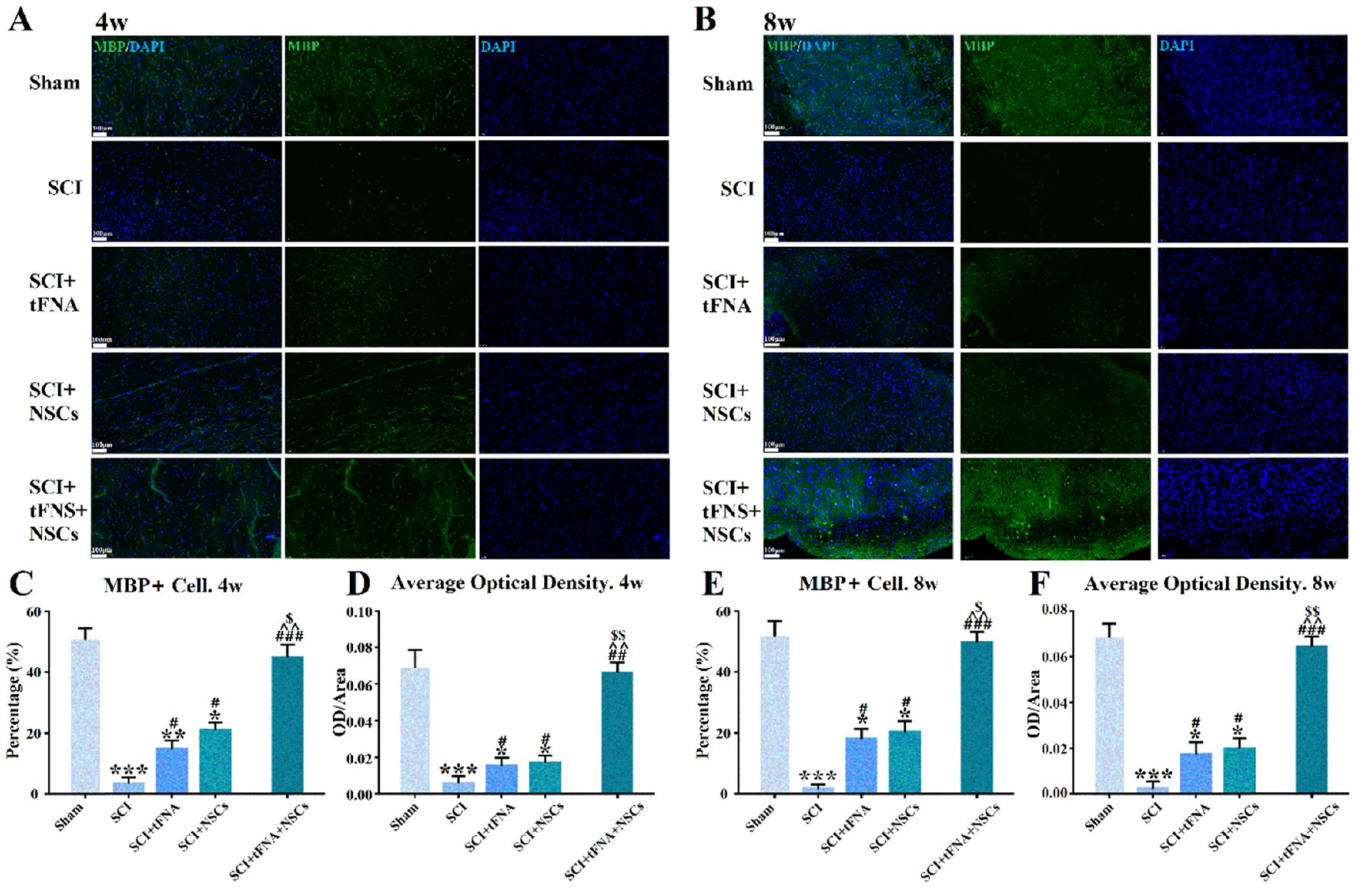

Figure 8. Immunohistochemistry of MBP protein in the lesion sites of each group. (A) Immunohistochemistry images of MBP protein in the lesion sites of SCI model rats after 4 week treatment. Scale bars are 100 μm. (B) Immunohistochemistry images of MBP protein in the lesion sites of SCI model rats after 8 week treatment. Scale bars are 100 μm. (C) Statistical analysis of the percentage of MBP-positive cells in the lesion sites of SCI model rats after 4 week treatment. Data are presented as mean ± SD (n = 3). Statistical analysis: $^{*}p < 0.05$, $^{**}p < 0.01$, $^{***}p < 0.001$ versus sham; $^{\#}p < 0.05$, $^{\#\#\#}p < 0.001$ versus SCI; $\wedge\wedge p < 0.01$ versus SCI+tFNA; $^{\$}p < 0.05$ versus SCI+NSCs. (D) Quantification of the average optical density of the MBP in the lesion sites of SCI model rats after 4 week treatment. Data are presented as mean ± SD (n = 3). Statistical analysis: $^{*}p < 0.05$, $^{***}p < 0.001$ versus sham; $^{\#}p < 0.05$, $^{\#\#}p < 0.01$ versus SCI; $\wedge\wedge p < 0.01$ versus SCI+tFNA; $^{\$\$}p < 0.01$ versus SCI+NSCs. (E) Statistical analysis of the percentage of MBP-positive cells in the lesion sites of SCI model rats after 8 week treatment. Data are presented as mean ± SD (n = 3). Statistical analysis: $^{*}p < 0.05$, $^{***}p < 0.001$ versus sham; $^{\#}p < 0.05$, $^{\#\#\#}p < 0.001$ versus SCI; $\wedge\wedge p < 0.01$ versus SCI+tFNA; $^{\$}p < 0.05$ versus SCI+NSCs. (F) Quantification of the average optical density of the MBP in the lesion sites of SCI model rats after 8 week treatment. Data are presented as mean ± SD (n = 3). Statistical analysis: $^{*}p < 0.05$, $^{***}p < 0.001$ versus sham; $^{\#}p < 0.05$, $^{\#\#\#}p < 0.001$ versus SCI; $\wedge\wedge p < 0.01$ versus SCI+tFNA; $^{\$\$}p < 0.01$ versus SCI+NSCs.

astrocytes, which could decrease the formation of glial scar. Therefore, the concomitant treatment of tFNA and NSCs manifested great potential in serving as an effective therapeutic aid in the neural regeneration of SCI.

EXPERIMENTAL SECTION

Preparation and Characterization of tFNA. The details about how the tFNA was generated have been well described in our previous studies.[39−42,57] Briefly, each single-stranded DNA (ssDNA; TaKaRa, Ostu, Japan; Table 1) was added to the TM buffer ($MgCl_2$ 50 nM, Tris-HCl 10 nM, pH = 8.0) equally, blended well, heated to 95 °C (10 min), and cooled to 4 °C (30 min). Capillary gel electrophoresis (CGE; Bioptic, Qsep100 Advance, Taiwan, China) was applied to measure the length of each ssDNA and tFNA. We also used PAGE (8%, Biotime, Nanjing, China) to testify the successful generation of tFNA. We adopted DLS to measure the size and PDI of tFNA. Then, the morphology of tFNA was also investigated by TEM (Libra 200, Zeiss, Germany) and AFM (SPM-9700 instrument, Japan). In the experiment of TEM, the sample was spread on a copper sheet without any stain and dried under infrared light for 5 min and tested using a microscope. As for the test in AFM, tFNA was dropped on a sheet, dried in the air circulation place, and then measured by AFM.

Animal Models. All adult female Sprague−Dawley (SD) rats with a weight of 240−260 g were bought from the Chinese Academy of Science, Sichuan Branch (Sichuan, China). Pregnant female SD rats were prepared for collecting fetal NSCs on the embryonic 10th−12th day. All rats were fed with rodent food and water under standard conditions. All animal experiments were conducted according to the guidelines of the animal ethics committee of Sichuan University.

Isolation and Culture of NSCs. Fetal rats were obtained from pregnant rats on the embryonic 10th−12th day. All brains of anesthetized sucking rats were dissected and minced under the sterile surgical condition, and the primary NSCs were isolated from the brain tissue mainly after the separation of meninx and cerebral vessels. All minced brains were digested with 0.05% trypsin for 15 min. Then, 200 mesh sieves were used to remove the undigested tissue, and the filtrate was centrifuged at 1000 r/min for 5 min to remove the residual trypsin. After that, cells were resuspended and incubated with complete DMEM/F12 medium supported with basic fibroblast growth factor (bFGF; 20 ng/mL, Gibco), epidermal growth factor (EGF; 20 ng/mL, Gibco), N2 supplement (10 ng/mL, Sigma), and B12 supplement (20 ng/mL, Sigma). The NSCs were passaged once a

DOI: 10.1021/acsami.9b19079
ACS Appl. Mater. Interfaces 2020, 12, 2095−2106

week for two to four generations to collect more stem cells for transplantation.

Identification of NSCs. Nestin, an important predominant biomarker protein of progenitor/stem cells, was used to examine whether the cultured cells were NSCs based on their abilities of proliferation and differentiation. The fourth-generation NSCs were seeded on plates in growth medium supplemented with 5% fetal calf serum (FCS; Corning) for 24 h, which was exposed on 0.01% poly-L-ornithine for 24 h. Cells were washed thrice with phosphate-buffered saline (PBS), fixed in paraformaldehyde for 30 min at 4 °C, and treated with Triton X-100 for 10 min at 37 °C. Then, cells were blocked with sheep serum for 1 h at 37 °C. Subsequently, we treated cells with primary antibody (anti-Nestin, Abcom) overnight. On the next day, we removed the primary antibody and treated cells with the secondary antibody for 1 h at 37 °C. The cytoskeleton and nucleus were then labeled with phalloidin for 1 h and 4′,6-diamidino-2-phenylindole (DAPI) for 10 min, respectively. Finally, all samples were tested by a fluorescence microscope (OLYMPUS CK31, Japan).

Cellular Uptake of tFNA by NSCs. In our previous studies, we had found that tFNA could enter various cells, including adipose-derived stem cells (ADSCs), chondrocyte, and some tumor cells. In this study, it is also a significant precondition for tFNA to enter NSCs before exerting its biological effects on NSCs. Therefore, the confocal imaging and flow cytometry were used to analyze the cell uptake of Cy5-tFNA. NSCs were plated on dishes preprocessed with 0.01% poly-L-ornithine for 24 h. After 24 h incubation, cells were treated with Cy5-tFNA for 12 h. All cells were washed thrice with PBS to remove the residual Cy5-tFNA, fixed with paraformaldehyde for 30 min at 4 °C, and stained with phalloidine and DAPI. Finally, all samples were tested by a laser confocal microscope (N-SIM, Nikon, Japan). For flow cytometry, NSCs were seeded on 6-well plates for 24 h and then exposed to Cy5-tFNA for 12 h. Cells were rinsed with PBS three times, harvested in PBS, and tested by a flow cytometer (Beckman Coulter, Cytomics FC 500, USA).

Blood Circulation and In vivo Distribution of tFNA. One hundred microliters Cy5-tFNA (1 μM) was injected into nude mice (male, 20 g, 6 week-old, Balb/c) by tail vein injection to measure the blood circulation time and observe the in vivo distribution of tFNA. Before that, all mice were anesthetized by 10% chloral hydrate (100 μL/mouse) and then were imaged with a whole-body fluorescence system (QuickView3000, Bio-Real, Austria) at different time points (i.e., before injection and 5, 15, 30, 45, and 60 min after injection).

Proliferation of NSCs by Brdu Straining and Flow Cytometry. In order to determine whether tFNA could affect the proliferation of NSCs, we used Brdu to mark the newly synthesized DNA, which would increase significantly if the proliferation of NSCs was promoted. Brdu is a kind of nucleic acid analogue, which can be used as a raw material for the synthesis of DNA in cells with proliferating ability. Brdu can also be recognized by some specific antibodies thus could be used to mark the cells that have the newly generated DNA. In this investigation, NSCs were seeded in dishes for 24 h, which were embedded with 0.01% poly-L-ornithine for 24 h. Then, cells were cultured with 250 nM tFNA and BrdU for 24 h. All cells were fixed in paraformaldehyde for 30 min at 4 °C, permeabilizated by 0.05% Triton-X for 10 min, blocked by 20% sheep serum for 1 h, and incubated with the primary antibody (anti-Brdu, Abcom) overnight at 4 °C. On the second day, all cell samples were treated with the second antibody for 1 h. The cells were stained with DAPI for 10 min. Finally, all samples were tested by a light microscope (Nikon, Japan).

To further observe the proliferation of NSCs, we also conducted the flow cytometry to measure the effects of tFNA on the cell cycle. NSCs were seeded on culture flasks (25 cm^2 surface area, Corning) and culture plates for 24 h, treated with 250 nM tFNA for 24 h, and harvested by PBS. The cells were washed by PBS three times and kept in cold ethanol overnight at −20 °C. In the following day, all cell samples were treated with RNase (100 μL) at 37 °C for 30 min and incubated with propidium iodide (PI; 400 μL) for 30 min at 4 °C in the dark. Finally, all samples were determined by a flow cytometer (FC500 Beckman, IL, USA).

Model Establishment of Spinal Cord Injury and Experimental Design. A hemisected spinal cord injury surgery was conducted on adult SD rats. Sodium pentobarbital (1%, 40 μg/g) was used to anesthetize healthy rats, and then a T9 hemisected spinal cord injury was made in model rats. Briefly, the skin of rats was shaved and disinfected with a betadine solution, then the skin was incised, and the muscle tissue was separated to unclose the T8-T10 vertebral body. The laminectomy was conducted at T9 to show the half-cut spinal cord. After a longitudinal incision preformed in the dura to expose the posterior median sulcus, the right half of the spinal cord was cut at T9 followed by the removal of a 2 mm segment. Then, the soft tissue was sutured individually, and animal post-operative care was required to avoid autophagia and infection, including bowel care and proper bladder. All rats in the study were randomly divided into five groups: (i) sham-operated group: laminectomy without SCI; (ii) control group: half-cut spinal cord injury with NS treatment; (iii) tFNA group: half-cut spinal cord injury with 250 nM tFNA treatment; (iv) NSCs group: half-cut spinal cord injury with NSCs treatment; and (v) tFNA+NSCs group: half-cut spinal cord injury with combined tFNA and NSCs treatment. Every group has nine rats with the successful modeling of SCI. The successful modeling of SCI was tested by the BBB scores.

Treatment of Different Groups. After 7 days of the SCI operation, different treatments were administered to rats via located injection at the spinal dural of T9. In the tFNA-treated group, 50 μL/mice (250 nM) tFNA was injected into rats for 2 weeks. In the NSCs-treated group, 5 μL/mice/d NSCs (1×10^5/μL in NS) was transplanted into the injured T9 with a speed of 0.5 μL/min. In the combined tFNA+NSCs-treated group, after the NSCs were injected into rats, the 50 μL/mice/d (250 nM) tFNA was injected into rats for 2 weeks. In the sham-operated group and control group, 50 μL/mice/d NS was injected into rats with the same frequency.

Basso−Beattie−Bresnahan (BBB) Ratings. The ratings of BBB scale are determined according to the hindlimb locomotor function. The tests were conducted before the SCI operation and after from 12 h to 8 weeks. In the BBB ratings, the rats were placed and allowed to move freely on an open field for 5 min individually. Two experienced raters assessed the performance of each rat according to the BBB scale while being blinded to the groups. The BBB scale ranges from 0 (no limb movement or weight support) to 21 (normal locomotion).

TUNEL Staining. Four and 8 weeks later after SCI operation, the tissue of SCI was separated from the spinal cord and fixed in 4% paraformaldehyde for 24 h. All tissue was dehydrated using graded ethanol as follows: 75% ethanol for 1 h, 85% ethanol for 1 h, 90% ethanol for 1 h, 95% ethanol for 1 h, and absolute ethyl acohol for 1 h. Then, the tissue was vitrified by dimethylbenzene for 20 min and paraffin-embedded. Then, the paraffin-embedded tissue was treated with dimethylbenzene for 1 h and dehydrated using graded ethanol as follows: absolute ethyl acohol for 20 min, 95% ethanol for 10 min, 90% ethanol for 5 min, 80% ethanol for 5 min, and 70% ethanol for 5 min. Next, after being treated with proteinase K (20 μg/mL) without DNase, all tissue samples were stained with TUNEL solution for 1 h at 37 °C, washed with PBS thrice, and treated with DAPI (1:1000, Sigma) for 10 min. Finally, all images of samples were captured by a laser scanning confocal microscope (Nikon-SN, Japan). The apoptotic index of all rat groups was also calculated and compared among them.

Histology. At ends of fourth and eight week after injury of rats, the histological evaluation was also conducted. The T7-T11 spinal cord pieces of euthanized rats were separated and fixed in 4% paraformaldehyde for 24 h, and the spinal cord sections were prepared as mentioned above in TUNEL staining. Then, cross-sectional or longitudinal sections of the spinal cord were made and dyed with hematoxylin and eosin (H&E) to assess the tissue histology and damage. Finally, the images of H&E were captured by a microscope (Lisa).

Immunohistochemistry. In immunohistochemistry, the spinal cord sections were prepared as mentioned above in TUNEL staining. All sections were blocked with 5% BSA (serum) for 30 min and incubated with primary antibodies (anti-GFAP, anti-MBP, anti-nestin, and anti-Neun) overnight at 4 °C. On the next day, the sections were

DOI: 10.1021/acsami.9b19079
ACS Appl. Mater. Interfaces 2020, 12, 2095−2106

treated with the secondary antibodies for 1 h at 37 °C and dyed with DAPI for 10 min. During each step, all samples were washed with PBS thrice for 5 min. Finally, the immunohistochemistry samples were observed with a laser scanning confocal microscope (Nikon-SN, Japan).

Amino Cupric Silver Staining. After 7 weeks of SCI, the amino cupric silver was injected into the peroneal nerve for the assessment of neuronal and axonal degeneration and function. The samples were treated in the same way as mentioned above in TUNEL staining, and all images were taken by a laser scanning confocal microscope (Nikon-SN, Japan).

Statistical Analysis. All experiments were performed for more than three times, and the experimental data were presented as mean ± standard deviation (SD) and analyzed with GraphPad (version 7.0). One-way analysis of variance (ANOVA) was adopted to compare the variables among groups. The differences in BBB scores among all rat groups were evaluated with repeated-measures ANOVA.

AUTHOR INFORMATION

Corresponding Author

*E-mail: yunfenglin@scu.edu.cn. Tel: 86-28-85503487. Fax: 86-28-85503487.

ORCID

Yunfeng Lin: 0000-0003-1224-6561

Author Contributions

†W.M. and Y.Z. contributed equally to this work.

Notes

The authors declare no competing financial interest.

ACKNOWLEDGMENTS

This study was supported by the National Key R&D Program of China (2019YFA0110600) and National Natural Science Foundation of China (81970916, 81671031). We are grateful to Dr. Chenghui Li (Analytical and Testing Center, Sichuan University) for her help in capturing the laser scanning confocal images and assisting with the particle size analysis.

REFERENCES

(1) Wang, X.-J.; Peng, C.-H.; Zhang, S.; Xu, X.-L.; Shu, G.-F.; Qi, J.; Zhu, Y.-F.; Xu, D.-M.; Kang, X.-Q.; Lu, K.-J.; Jin, F.-Y.; Yu, R.-S.; Ying, X.-Y.; You, J.; Du, Y.-Z.; Ji, J.-S. Polysialic-Acid-Based Micelles Promote Neural Regeneration in Spinal Cord Injury Therapy. *Nano Lett.* **2019**, *19*, 829−838.

(2) Li, X.; Wu, M.; Gu, L.; Ren, Y.; Mu, M.; Wang, Y.; Gao, X.; Li, J.; Tong, A.; Zhu, H.; Zhou, L.; Chen, H.; Guo, G. A single dose of thermal-sensitive biodegradable hybrid hydrogel promotes functional recovery after spinal cord injury. *Appl. Mater. Today* **2019**, *14*, 66−75.

(3) Banaszek, D.; Inglis, T.; Marion, T. E.; Charest-Morin, R.; Moskven, E.; Rivers, C. S.; Kurban, D.; Flexman, A. M.; Ailon, T.; Dea, N.; Kwon, B. K.; Paquette, S.; Fisher, C. G.; Dvorak, M. F.; Street, J. T. Effect of Frailty on Outcome after Traumatic Spinal Cord Injury. *J. Neurotrauma.* **2019**, DOI: 10.1089/neu.2019.6581.

(4) Belin, S.; Nawabi, H.; Wang, C.; Tang, S.; Latremoliere, A.; Warren, P.; Schorle, H.; Uncu, C.; Woolf, C. J.; He, Z.; Steen, J. A. Injury-induced decline of intrinsic regenerative ability revealed by quantitative proteomics. *Neuron* **2015**, *86*, 1000−1014.

(5) Slotkin, J. R.; Pritchard, C. D.; Luque, B.; Ye, J.; Layer, R. T.; Lawrence, M. S.; O'Shea, T. M.; Roy, R. R.; Zhong, H.; Vollenweider, I.; Edgerton, V. R.; Courtine, G.; Woodard, E. J.; Langer, R. Biodegradable scaffolds promote tissue remodeling and functional improvement in non-human primates with acute spinal cord injury. *Biomaterials* **2017**, *123*, 63−76.

(6) Gu, S.; Shen, Y.; Xu, W.; Xu, L.; Li, X.; Zhou, G.; Gu, Y.; Xu, J. Application of fetal neural stem cells transplantation in delaying denervated muscle atrophy in rats with peripheral nerve injury. *Microsurgery* **2010**, *30*, 266−274.

(7) Płatek, R.; Grycz, K.; Więkowska, A.; Czarkowska-Bauch, J.; Skup, M. L1 Cell Adhesion Molecule overexpression down regulates phosphacan and up regulates structural plasticity-related genes rostral and caudal to the complete spinal cord transection. *J. Neurotrauma.* **2019**, DOI: 10.1089/neu.2018.6103.

(8) Terenzio, M.; Koley, S.; Samra, N.; Rishal, I.; Zhao, Q.; Sahoo, P. K.; Urisman, A.; Marvaldi, L.; Oses-Prieto, J. A.; Forester, C.; Gomes, C.; Kalinski, A. L.; Di Pizio, A.; Doron-Mandel, E.; Perry, R. B.-T.; Koppel, I.; Twiss, J. L.; Burlingame, A. L.; Fainzilber, M. Locally translated mTOR controls axonal local translation in nerve injury. *Science* **2018**, *359*, 1416−1421.

(9) Bradbury, E. J.; Moon, L. D. F.; Popat, R. J.; King, V. R.; Bennett, G. S.; Patel, P. N.; Fawcett, J. W.; McMahon, S. B. Chondroitinase ABC promotes functional recovery after spinal cord injury. *Nature* **2002**, *416*, 636−640.

(10) Khankan, R. R.; Griffis, K. G.; Haggerty-Skeans, J. R.; Zhong, H.; Roy, R. R.; Edgerton, V. R.; Phelps, P. E. Olfactory Ensheathing Cell Transplantation after a Complete Spinal Cord Transection Mediates Neuroprotective and Immunomodulatory Mechanisms to Facilitate Regeneration. *J. Neurosci.* **2016**, *36*, 6269−6286.

(11) Mahar, M.; Cavalli, V. Intrinsic mechanisms of neuronal axon regeneration. *Nat. Rev. Neurosci.* **2018**, *19*, 323−337.

(12) Ruschel, J.; Hellal, F.; Flynn, K. C.; Dupraz, S.; Elliott, D. A.; Tedeschi, A.; Bates, M.; Sliwinski, C.; Brook, G.; Dobrindt, K.; Peitz, M.; Brüstle, O.; Norenberg, M. D.; Blesch, A.; Weidner, N.; Bunge, M. B.; Bixby, J. L.; Bradke, F. Systemic administration of epothilone B promotes axon regeneration after spinal cord injury. *Science* **2015**, *348*, 347−352.

(13) Hosseini, S. R.; Kaka, G.; Joghataei, M. T.; Hooshmandi, M.; Sadraie, S. H.; Yaghoobi, K.; Mansoori, K.; Mohammadi, A. Coadministration of Dexamethasone and Melissa officinalis Has Neuroprotective Effects in Rat Animal Model with Spinal Cord Injury. *Cell J.* **2017**, *19*, 102−116.

(14) Kiwerski, J. E. Application of dexamethasone in the treatment of acute spinal cord injury. *Injury* **1993**, *24*, 457−460.

(15) Vaquero, J.; Zurita, M. Tissue expression of 165-aa vascular permeability factor after spinal cord injury is not influenced by dexamethasone administration in rats. *Neurosci. Lett.* **2004**, *365*, 214−217.

(16) Wang, Z.; Zhou, L.; Zheng, X.; Liu, W. Effects of dexamethasone on autophagy and apoptosis in acute spinal cord injury. *Neuroreport* **2018**, *29*, 1084−1091.

(17) Bracken, M. B.; Shepard, M. J.; Holford, T. R.; Leo-Summers, L.; Aldrich, E. F.; Fazl, M.; Fehlings, M.; Herr, D. L.; Hitchon, P. W.; Marshall, L. F.; Nockels, R. P.; Pascale, V.; Perot, P. L., Jr.; Piepmeier, J.; Sonntag, V. K. H.; Wagner, F.; Wilberger, J. E.; Winn, H. R.; Young, W. Administration of methylprednisolone for 24 or 48 hours or tirilazad mesylate for 48 hours in the treatment of acute spinal cord injury. Results of the Third National Acute Spinal Cord Injury Randomized Controlled Trial. National Acute Spinal Cord Injury Study. *JAMA* **1997**, *277*, 1597−1604.

(18) Cerqueira, S. R.; Oliveira, J. M.; Silva, N. A.; Leite-Almeida, H.; Ribeiro-Samy, S.; Almeida, A.; Mano, J. F.; Sousa, N.; Salgado, A. J.; Reis, R. L. Microglia response and in vivo therapeutic potential of methylprednisolone-loaded dendrimer nanoparticles in spinal cord injury. *Small* **2013**, *9*, 738−749.

(19) Baglio, S. R.; Rooijers, K.; Koppers-Lalic, D.; Verweij, F. J.; Lanzón, M. P.; Zini, N.; Naaijkens, B.; Perut, F.; Niessen, H. W. M.; Baldini, N.; Pegtel, D. M. Human bone marrow- and adipose-mesenchymal stem cells secrete exosomes enriched in distinctive miRNA and tRNA species. *Stem Cell Res. Ther.* **2015**, *6*, 127.

(20) Phinney, D. G.; Pittenger, M. F. Concise Review: MSC-Derived Exosomes for Cell-Free Therapy. *Stem Cells* **2017**, *35*, 851−858.

(21) Zhang, Z. G.; Buller, B.; Chopp, M. Exosomes - beyond stem cells for restorative therapy in stroke and neurological injury. *Nat. Rev. Neurol.* **2019**, *15*, 193−203.

(22) Haney, M. J.; Klyachko, N. L.; Zhao, Y.; Gupta, R.; Plotnikova, E. G.; He, Z.; Patel, T.; Piroyan, A.; Sokolsky, M.; Kabanov, A. V.;

DOI: 10.1021/acsami.9b19079
ACS Appl. Mater. Interfaces 2020, 12, 2095−2106

Batrakova, E. V. Exosomes as drug delivery vehicles for Parkinson's disease therapy. *J. Controlled Release* **2015**, *207*, 18−30.
(23) Reza-Zaldivar, E. E.; Hernández-Sapiéns, M. A.; Minjarez, B.; Gutiérrez-Mercado, Y. K.; Márquez-Aguirre, A. L.; Canales-Aguirre, A. A. Potential Effects of MSC-Derived Exosomes in Neuroplasticity in Alzheimer's Disease. *Front. Cell. Neurosci.* **2018**, *12*, 317.
(24) Fouad, H.; Al-Shammari, B. A.; AlRez, M. F.; Al-Fotawi, R.; Mahmood, A. Modified Bi-Layered Polycaprolactone Nanofiber Scaffolds for Vascular Tissue Engineering Applications. *Nanosci. Nanotechnol. Lett.* **2019**, *11*, 1−10.
(25) Shu, J.; Mo, S.; Wen, Q.; Qin, Y.; Jiang, L. Study on Immune Regulation of Bone Marrow Mesenchymal Stem Cell-Derived Exosomes in Preterm Infants with Brain Injury. *Nanosci. Nanotechnol. Lett.* **2018**, *10*, 1598−1605.
(26) Chao, J.; Wang, J.; Wang, F.; Ouyang, X.; Kopperger, E.; Liu, H.; Li, Q.; Shi, J.; Wang, L.; Hu, J.; Wang, L.; Huang, W.; Simmel, F. C.; Fan, C. Solving mazes with single-molecule DNA navigators. *Nat. Mater.* **2019**, 273.
(27) Han, Y.; Li, X.; Chen, H.; Hu, X.; Luo, Y.; Wang, T.; Wang, Z.; Li, Q.; Fan, C.; Shi, J.; Wang, L.; Zhao, Y.; Wu, C.; Chen, N. Real-Time Imaging of Endocytosis and Intracellular Trafficking of Semiconducting Polymer Dots. *ACS Appl. Mater. Interfaces* **2017**, *9*, 21200−21208.
(28) Lin, M.; Song, P.; Zhou, G.; Zuo, X.; Aldalbahi, A.; Lou, X.; Shi, J.; Fan, C. Electrochemical detection of nucleic acids, proteins, small molecules and cells using a DNA-nanostructure-based universal biosensing platform. *Nat. Protoc.* **2016**, *11*, 1244−1263.
(29) Liu, B.; Song, C.; Zhu, D.; Wang, X.; Zhao, M.; Yang, Y.; Zhang, Y.; Su, S.; Shi, J.; Chao, J.; Liu, H.; Zhao, Y.; Fan, C.; Wang, L. DNA-Origami-Based Assembly of Anisotropic Plasmonic Gold Nanostructures. *Small* **2017**, *13*, 1603991.
(30) Liu, X.; Zhang, F.; Jing, X.; Pan, M.; Liu, P.; Li, W.; Zhu, B.; Li, J.; Chen, H.; Wang, L.; Lin, J.; Liu, Y.; Zhao, D.; Yan, H.; Fan, C. Complex silica composite nanomaterials templated with DNA origami. *Nature* **2018**, *559*, 593−598.
(31) Madhanagopal, B. R.; Zhang, S.; Demirel, E.; Wady, H.; Chandrasekaran, A. R. DNA Nanocarriers: Programmed to Deliver. *Trends Biochem. Sci.* **2018**, *43*, 997−1013.
(32) Xie, X.; Shao, X.; Ma, W.; Zhao, D.; Shi, S.; Li, Q.; Lin, Y. Overcoming drug-resistant lung cancer by paclitaxel loaded tetrahedral DNA nanostructures. *Nanoscale* **2018**, *10*, 5457−5465.
(33) Ma, W.; Zhan, Y.; Zhang, Y.; Shao, X.; Xie, X.; Mao, C.; Cui, W.; Li, Q.; Shi, J.; Li, J.; Fan, C.; Lin, Y. An Intelligent DNA Nanorobot with in Vitro Enhanced Protein Lysosomal Degradation of HER2. *Nano Lett.* **2019**, *19*, 4505−4517.
(34) Zhan, Y.; Ma, W.; Zhang, Y.; Mao, C.; Shao, X.; Xie, X.; Wang, F.; Liu, X.; Li, Q.; Lin, Y. DNA-Based Nanomedicine with Targeting and Enhancement of Therapeutic Efficacy of Breast Cancer Cells. *ACS Appl. Mater. Interfaces* **2019**, *11*, 15354−15365.
(35) Zhang, Y.; Ma, W.; Zhu, Y.; Shi, S.; Li, Q.; Mao, C.; Zhao, D.; Zhan, Y.; Shi, J.; Li, W.; Wang, L.; Fan, C.; Lin, Y. Inhibiting Methicillin-Resistant Staphylococcus aureus by Tetrahedral DNA Nanostructure-Enabled Antisense Peptide Nucleic Acid Delivery. *Nano Lett.* **2018**, *18*, 5652−5659.
(36) Meng, L.; Ma, W.; Lin, S.; Shi, S.; Li, Y.; Lin, Y. Tetrahedral DNA Nanostructure-Delivered DNAzyme for Gene Silencing to Suppress Cell Growth. *ACS Appl. Mater. Interfaces* **2019**, *11*, 6850−6857.
(37) Tian, T.; Zhang, T.; Zhou, T.; Lin, S.; Shi, S.; Lin, Y. Synthesis of an ethyleneimine/tetrahedral DNA nanostructure complex and its potential application as a multi-functional delivery vehicle. *Nanoscale* **2017**, *9*, 18402−18412.
(38) Li, X.; Xie, X.; Ma, Z.; Li, Q.; Liu, L.; Hu, X.; Liu, C.; Li, B.; Wang, H.; Chen, N.; Fan, C.; Song, H. Programming Niche Accessibility and In Vitro Stemness with Intercellular DNA Reactions. *Adv. Mater.* **2018**, *30*, 1804861.
(39) Ma, W.; Shao, X.; Zhao, D.; Li, Q.; Liu, M.; Zhou, T.; Xie, X.; Mao, C.; Zhang, Y.; Lin, Y. Self-Assembled Tetrahedral DNA Nanostructures Promote Neural Stem Cell Proliferation and Neuronal Differentiation. *ACS Appl. Mater. Interfaces* **2018**, *10*, 7892−7900.
(40) Ma, W.; Xie, X.; Shao, X.; Zhang, Y.; Mao, C.; Zhan, Y.; Zhao, D.; Liu, M.; Li, Q.; Lin, Y. Tetrahedral DNA nanostructures facilitate neural stem cell migration via activating RHOA/ROCK2 signalling pathway. *Cell Prolif.* **2018**, *51*, No. e12503.
(41) Shao, X.; Ma, W.; Xie, X.; Li, Q.; Lin, S.; Zhang, T.; Lin, Y. Neuroprotective Effect of Tetrahedral DNA Nanostructures in a Cell Model of Alzheimer's Disease. *ACS Appl. Mater. Interfaces* **2018**, *10*, 23682−23692.
(42) Shao, X.; Lin, S.; Peng, Q.; Shi, S.; Wei, X.; Zhang, T.; Lin, Y. Tetrahedral DNA Nanostructure: A Potential Promoter for Cartilage Tissue Regeneration via Regulating Chondrocyte Phenotype and Proliferation. *Small* **2017**, *13*, 1602770.
(43) Shi, S.; Lin, S.; Li, Y.; Zhang, T.; Shao, X.; Tian, T.; Zhou, T.; Li, Q.; Lin, Y. Effects of tetrahedral DNA nanostructures on autophagy in chondrocytes. *Chem. Commun.* **2018**, *54*, 1327−1330.
(44) Zhang, Q.; Lin, S.; Shi, S.; Zhang, T.; Ma, Q.; Tian, T.; Zhou, T.; Cai, X.; Lin, Y. Anti-inflammatory and Antioxidative Effects of Tetrahedral DNA Nanostructures via the Modulation of Macrophage Responses. *ACS Appl. Mater. Interfaces* **2018**, *10*, 3421−3430.
(45) Song, R. B.; Basso, D. M.; da Costa, R. C.; Fisher, L. C.; Mo, X.; Moore, S. A. Adaptation of the Basso-Beattie-Bresnahan locomotor rating scale for use in a clinical model of spinal cord injury in dogs. *J. Neurosci. Methods* **2016**, *268*, 117−124.
(46) Barros Filho, T. E. P. D.; Molina, A. E. I. S. Analysis of the sensitivity and reproducibility of the Basso, Beattie, Bresnahan (BBB) scale in Wistar rats. *Clinics* **2008**, *63*, 103−108.
(47) Baetas-da-Cruz, W.; Macedo-Silva, R. M.; Santos-Silva, A.; Henriques-Pons, A.; Madeira, M. F.; Corte-Real, S.; Cavalcante, L. A. Destiny and intracellular survival of Leishmania amazonensis in control and dexamethasone-treated glial cultures: protozoa-specific glycoconjugate tagging and TUNEL staining. *J. Histochem. Cytochem.* **2004**, *52*, 1047−1055.
(48) Fu, Y.-B.; Ahmed, Z.; Yang, H.; Horbach, C. TUNEL Assay and DAPI Staining Revealed Few Alterations of Cellular Morphology in Naturally and Artificially Aged Seeds of Cultivated Flax. *Plants* **2018**, *7*, 24.
(49) Seigel, G. M.; Ambati, J.; Richard Green, W.; McDaniel, T. V. Ice incubation step allows adherence of archival histological specimens on gelatin-coated slides for TUNEL staining. *Brain Res. Protoc.* **1998**, *3*, 119−122.
(50) Andressen, C.; Stöcker, E.; Klinz, F.-J.; Lenka, N.; Hescheler, J.; Fleischmann, B.; Arnhold, S.; Addicks, K. Nestin-specific green fluorescent protein expression in embryonic stem cell-derived neural precursor cells used for transplantation. *Stem Cells* **2001**, *19*, 419−424.
(51) Ernst, C.; Christie, B. R. The putative neural stem cell marker, nestin, is expressed in heterogeneous cell types in the adult rat neocortex. *Neuroscience* **2006**, *138*, 183−188.
(52) Wang, J.; Huang, Y.; Cai, J.; Ke, Q.; Xiao, J.; Huang, W.; Li, H.; Qiu, Y.; Wang, Y.; Zhang, B.; Wu, H.; Zhang, Y.; Sui, X.; Bardeesi, A. S. A.; Xiang, A. P. A Nestin-Cyclin-Dependent Kinase 5-Dynamin-Related Protein 1 Axis Regulates Neural Stem/Progenitor Cell Stemness via a Metabolic Shift. *Stem Cells* **2018**, *36*, 589−601.
(53) Cascante, A.; Klum, S.; Biswas, M.; Antolin-Fontes, B.; Barnabé-Heider, F.; Hermanson, O. Gene-specific methylation control of H3K9 and H3K36 on neurotrophic BDNF versus astroglial GFAP genes by KDM4A/C regulates neural stem cell differentiation. *J. Mol. Biol.* **2014**, *426*, 3467−3477.
(54) Imura, T.; Kornblum, H. I.; Sofroniew, M. V. The predominant neural stem cell isolated from postnatal and adult forebrain but not early embryonic forebrain expresses GFAP. *J. Neurosci.* **2003**, *23*, 2824−2832.
(55) Raponi, E.; Agenes, F.; Delphin, C.; Assard, N.; Baudier, J.; Legraverend, C.; Deloulme, J.-C. S100B expression defines a state in which GFAP-expressing cells lose their neural stem cell potential and acquire a more mature developmental stage. *Glia* **2007**, *55*, 165−177.

DOI: 10.1021/acsami.9b19079
ACS Appl. Mater. Interfaces 2020, 12, 2095−2106

(56) Chignola, R.; Cestari, T.; Guerriero, C.; Riviera, A. P.; Ferrari, S.; Brendolan, A.; Gobbo, M.; Amato, S.; Sartoris, S.; Fracasso, G.; Liuzzi, M. G.; Riccio, P.; Tridente, G.; Andrighetto, G. Expression of myelin basic protein (MBP) epitopes in human non-neural cells revealed by two anti-MBP IgM monoclonal antibodies. *Clin. Exp. Immunol.* **2000**, *122*, 429−436.
(57) Shi, S.; Peng, Q.; Shao, X.; Xie, J.; Lin, S.; Zhang, T.; Li, Q.; Li, X.; Lin, Y. Self-Assembled Tetrahedral DNA Nanostructures Promote Adipose-Derived Stem Cell Migration via lncRNA XLOC 010623 and RHOA/ROCK2 Signal Pathway. *ACS Appl. Mater. Interfaces* **2016**, *8*, 19353−19363.

DOI: 10.1021/acsami.9b19079
ACS Appl. Mater. Interfaces 2020, 12, 2095−2106